Pergamon

0956-7151(95)00177-8

Acta mater. Vol. 44, No. 2, pp. 725–734, 1996
Elsevier Science Ltd

1359-6454/96 $15.00 + 0.00

THE PHYSICS OF MECHANICAL ALLOYING IN A MODIFIED HORIZONTAL ROD MILL: MATHEMATICAL TREATMENT

M. ABDELLAOUI and E. GAFFET

CNRS-UPR A0423, "Far From Equilibrium Phase Transition Group",
Institut Polytechnique de Sévenans, F-90010 Belfort Cedex, France

(Received 20 December 1994; in revised form 22 March 1995)

Abstract—Based on kinematic modelling of the modified horizontal rod mill (MHRM), the kinematic equations giving the velocity and the acceleration of the rod in the cylinder of the mill are given. The kinetic energy transferred at the collision event, the shock frequency and the injected shock power are also calculated. Comparison of calculations to some prior experimental results confirms our assumption published in earlier works which states that neither the shock energy nor the shock frequency separately taken into account, govern the end product but only the injected shock power is responsible for the microstructure and phases present in the processed powder.

1. INTRODUCTION

Results from mechanical alloying (MA) are numerous. Formation of amorphous phase and intermetallics can be obtained by milling pure elements or elemental metal ribbons [1]. MA is also a technique for alloying non-miscible materials and for formation of supersaturated solid solutions [2–10]. The process is inherently flexible. So, it is reasonable to expect it to increase in importance. However, there has been little attempt to analyse it in a manner that would establish predictive capabilities for it, or at the least determine the physical parameters governing the phase transitions under the dynamical mechanical solicitation induced by milling.

Maurice and Courtney [11, 12] try to give an approach defining the geometry and the basic mechanics of the powder–work piece interaction for several common devices used for MA, since this information allows pertinent parameters of the process (e.g. impact velocity, powder material volume impacted, time between impacts, etc.) to be identified in terms of machine characteristics and process operating parameters. In the above-mentioned work, two configurations were considered—a vertical mill such as the szegvari attritor and a vibratory mill. The same author [13, 14] developed a model of mechanical alloying, applicable to a single collision event involving ductile species. R. W. Rydin *et al.* [15] studied the motion of grinding media and powder in an attritor canister by means of filming the agitated charge and frame-by-frame scrutiny of the footage.

Burgio *et al.* [16], by taking into account the influence of the ball radius, the ball mass and the number of balls, correlate the milling operating conditions and the powder end product in a "Fritsch Pulverisette P5" ball mill. The shock frequency was assumed to scale with the relative velocity ω_r ($\omega_r = \omega_v - \Omega_p$ with ω_v and Ω_p respectively the vial and the disk rotation speeds). Magini [17] states that the kinetic shock energy released by the ball into the powders is equal to the difference between the potential energies before and after the collision event of a ball on a flat surface.

We have reported in previous work [18, 19], based on a mathematical treatment of the mechanical alloying process in planetary ball mills and experimental results on the ball milled end product of the $Ni_{10}Zr_7$ compound, that neither the kinetic shock energy nor the shock frequency, taken separately, governs the end product. In other words, we show that only the mechanical injected shock power is responsible for the structural state of the end powder product.

The aim of this paper is to prove that, even when using a different device for milling (i.e. a modified horizontal rod mill), the assumption of the mechanical injected shock power controlling the structure of the processed powder remains true.

The purpose of this paper is thus to report the details of the mathematical treatment of the mechanical alloying in a modified horizontal rod mill (MHRM) and to compare experimental results with calculated predictions. As previously mentioned [18, 19], since the kinetic shock energy consumption has not been well defined previously, and to simplify the problem, the following assumptions are made in the numerical calculations

- the kinetic shock energy is released totally into the powders.

Other assumptions, which are justified later in the text, are

- there is not relative motion between the rod and the cylinder wall prior to the departure point, i.e. the rod does not slip or roll
- after the flight duration, the rod is newly attached to the wall.

2. MATHEMATICAL TREATMENT OF THE PROCESS TAKING PLACE IN A MODIFIED HORIZONTAL ROD MILL

In the approximation of collision in a planetary ball mill, McCormick *et al.* [20] have improved the basic model of Burgio *et al.* [16] by considering a "slip factor" that makes the trajectory of the flight ball rather different from the one calculated without considering this effect. Ball motion is recorded using a high speed video camera [20]. Le Brun *et al.* [21] confirmed this by a videotape recording of the trajectory-type. Rydin *et al.* [15] studied the motions of grinding media and powder in an attritor canister by means of filming the agitated charge and frame-by-frame scrutiny of the footage.

If the process taking place in planetary ball mills has been more or less previously studied, few experimental or theoretical studies have been done for the horizontal ball or rod mills. Maurice and Courtney [11] have carried out preliminary calculations of the ball impact velocity and the released kinetic shock energy in a classical horizontal ball mill. Calka *et al.* [22] have done some improvements of the horizontal mill geometry, i.e. the ball movement during the milling process is confined to the vertical plane by the cell walls and is controlled by an external magnetic field. The intensity and direction of the field are externally adjusted allowing the ball trajectories, impact energy and the shearing energy to be varied in a controlled manner.

In this section, rod motion in the cylindrical mill during one cycle is studied by taking into account the above-mentioned simplification assumptions. Thus, the coordinates of the rod, when it is stuck to the inner cylinder surface and after leaving the inner cylinder surface (detachment event), are calculated.

The application of the fundamental dynamic principle gives the rod detachment condition which allows calculation of the rod detachment position and detachment velocity. These latter parameters are used in order to calculate the motion of the rod from the detachment event up to the collision one.

The rod collision velocity gives the kinetic energy released from the rod to the powders. The time needed between two collision events or two detachment events gives the shock frequency.

The modelling of the MHRM is given in Fig. A1 and explained in paragraph A of the Appendix.

2.1. Absolute velocity and absolute acceleration of the rod before the detachment event

The adopted reference (O, **I**, **J**, **K**) to perform these calculations is a Cartesian one, with "O" the cylinder centre. The rod is illustrated by the material "M" point. Based on Fig. A1, the M point position is defined as

$$\mathbf{OM} = R\mathbf{U}_\rho = R[\cos(\theta)\mathbf{J} + \sin(\theta)\mathbf{K}]. \tag{1}$$

The absolute velocity $\mathbf{V}_a$ of the M point is given by the derivative of the **OM** vector [equation (1)] with respect to time. The final expression of the absolute velocity $\mathbf{V}_a$ and its amplitude are given in paragraph B of the Appendix as follows

$$\mathbf{V}_a = R\omega[-\sin(\theta)\mathbf{J} + \cos(\theta)\mathbf{K}] \tag{2}$$

$$\|\mathbf{V}_a\| = R\omega. \tag{3}$$

The absolute acceleration γ_a of the point M obtained by the derivative of its absolute velocity $\mathbf{V}_a$ with respect to time is

$$\gamma_a = -R\omega^2[\cos(\theta)\mathbf{J} + \sin(\theta)\mathbf{K}] \tag{4}$$

or along the $\mathbf{U}_\rho$ vector as

$$\gamma_a = -R\omega^2\mathbf{U}_\rho \tag{5}$$

its amplitude is given by

$$\|\gamma_a\| = R\omega^2. \tag{6}$$

2.2. Calculation of the detachment velocity and the detachment acceleration

To eliminate the slipping and/or the rolling between the rod and the inner cylinder wall, conventional horizontal rod mills are modified. In particular, a lifting system consisting of two fixed impellers, in opposite directions, on the right and the left mill covers is added. Figure A2 of the Appendix shows the front and a left side view of the modified horizontal rod mill (MHRM) with

(1) the cylinder
(2) impeller permitting lifting of the rod (lifting system)
(3) the rod used instead of the balls in the planetary ball mill
(4) two covers on which are fixed the impellers (one impeller on each cover).

Based on fundamental dynamics, the resultant of the external forces acting on the rod is equal to the product of its mass by its acceleration. The physical forces applied to the rod are its weight (gravitational action), the cylinder and the impellers reactions. In a reference frame fixed to the rod, the latter is considered fixed. So, the rod dynamic equilibrium is stipulated by

$$-m \cdot \gamma_a + \mathbf{R} + \mathbf{P} = \mathbf{0} \tag{7}$$

with **R** the cylinder and the impeller reactions and **P** the rod weight.

The resolution of equation (7) can be done easily by writing the rod weight, the impeller and the cylinder reactions as a function of the $\mathbf{U}_\rho$ and the $\mathbf{U}_\theta$ vectors. These calculations are developed in paragraph C of the Appendix. By combining equations (C1) and (C2) of the Appendix and equation (7), the following equations result

$$\mathbf{R}_\rho - mg\cos\left(\frac{\pi}{2}-\theta\right)\mathbf{U}_\rho + mR\omega^2\mathbf{U}_\rho = \mathbf{0} \quad (8)$$

$$\mathbf{R}_\theta - mg\sin\left(\frac{\pi}{2}-\theta\right)\mathbf{U}_\theta = 0 \quad (9)$$

with $\mathbf{R}_\rho$ the cylinder reaction and $\mathbf{R}_\theta$ the impeller reaction.

For detachment of the rod from the inner cylinder wall, equation (8) = 0; i.e.

$$-mg\cos\left(\frac{\pi}{2}-\theta_d\right)\mathbf{U}_\rho + mR\omega^2\mathbf{U}_\rho = \mathbf{0}. \quad (10a)$$

Equation (10a) can be simplified as

$$\sin(\theta_d) = \frac{R\omega^2}{g}. \quad (10b)$$

Taking into account the finite rod radius, equation (10b) becomes

$$\sin(\theta_d) = \frac{(R-r)\omega^2}{g}. \quad (10c)$$

The rod detachment angle θ_d and the rod detachment condition, corresponding to a revolution cylinder speed ω, are defined by equation (10c).

When the cylinder rotation speed $>\sqrt{g/R-r}$, detachment does not happen. the rod remains "stuck" to the inner cylinder surface.

2.3. Calculation of the collision point position

To obtain the time between the detachment and the collision events, a computer solution is utilised.

After detachment, the rod experiences only a gravitational force. Thus its trajectory conforms to that of a projectile, i.e. it is a parabola in the (O, Y, Z) plane materialised by the Cartesian referential (O, **J**, **K**). Its motion can be decomposed into two motions

(1) a uniform linear motion with a constant velocity $\mathbf{V}_{dy}$ and an initial position $\mathbf{OM}_{dy}$, in the horizontal direction
(2) an accelerated motion with an initial velocity $\mathbf{V}_{dz}$, an initial position $\mathbf{OM}_{dz}$ and an acceleration $\mathbf{g} = -g\mathbf{K}$, in the vertical direction.

Its motion expression at a "t" instant after the detachment event is

$$\mathbf{OM} = \tfrac{1}{2}\mathbf{g}t^2 + \mathbf{V}_d t + \mathbf{OM}_d = y\mathbf{J} + z\mathbf{K} \quad (11)$$

such as

$$y = (R-r)\cos(\theta_d) - (R-r)\omega\sin(\theta_d)t \quad (12)$$

$$z = -\tfrac{1}{2}gt^2 + (R-r)\omega\cos(\theta_d)t + (R-r)\sin(\theta_d). \quad (13)$$

Details are given in paragraph E of the Appendix.

The first collision between the rod and the inner cylinder surface occurs when the amplitude of the vector position **OM** becomes equal to the fictive radius $(R-r)$. So the collision condition is expressed as following

$$\sqrt{y^2+z^2} = (R-r). \quad (14)$$

The numerical approach consists of

(1) calculation of the angle detachment value (θ_d) [equation (9c)]
(2) increment time in steps "Δt" (μs)
(3) calculation of the "y" and "z" coordinates of the vector position **OM** [equations (12) and 13)]. If the collision condition [equation (14)] is fulfilled, the collision point coordinates values (y and z) along the "Y" and the "Z" axes and the time "t_c" needed between the detachment event and the collision event are determined.

2.4. Calculation of the kinetic energy by one hit

The kinetic impact energy is given by

$$E_k = \tfrac{1}{2}m\|\mathbf{V}_c\|^2. \quad (15)$$

The amplitude of the collision velocity (see paragraph F of the Appendix) is

$$\|\mathbf{V}_c\| = \sqrt{[(R-r)\omega\sin(\theta_d)]^2 + [-gt_c + (R-r)\omega\cos(\theta_d)]^2} \quad (16)$$

with m the rod mass, R the cylinder radius, r the rod radius, θ_d the detachment angle, ω the cylinder rotation speed, t_c the time between detachment and collision event and g the gravitational acceleration.

2.5. Calculation of the shock frequency

Following the collision event, the rod rolls on the inner cylinder surface until meeting the impellers (lifting system) which lifts it up to the detachment position.

During rolling on the cylinder surface, the rod interacts with the powder charge, deforming it further as well as causing fracture and welding of the particles within it. In order to simplify the problem, we do not consider these post-impact effects in our calculations; we consider only the collision effect.

The impact frequency is given only by the cylinder rotation speed since the geometrical construction

permits only one impact per cylinder revolution. It is given as follows

$$f = \frac{\omega}{2\pi} \tag{17}$$

with ω cylinder rotation speed expressed in rd s^{-1}. This shock frequency corresponds to one rod. So when operating with a given number of rods (N), the impact frequency is equal to the product of equation (17) and the number of rods in the mill corrected by a parameter accounting for interactions among the rods [16].

So as the cycle period, which is equal to a cylinder revolution period, is given by the sum of the flight duration, the rolling duration and the sticking period, the flight time does not give the shock frequency but it gives the rolling and the sticking periods.

2.6. Calculation of the shock power

The power released from the rod to the powders is the product of the frequency with the kinetic energy [18, 19]. It is given by

$$P = fE_k. \tag{18}$$

3. NUMERICAL CALCULATION RESULTS

The so-called MHRM has a 45 mm diameter and a 180 mm length. The calculations of the kinetic shock energy, the shock frequency and the shock power are carried out as a function of cylinder rotational velocity for different values of the rod radius. The calculations are carried out for only one rod. The hardened steel rods have a 150 mm length and a radius ranging from 7.5 up to 14.5 mm (the rod mass is 244 g for a 7.5 mm radius rod).

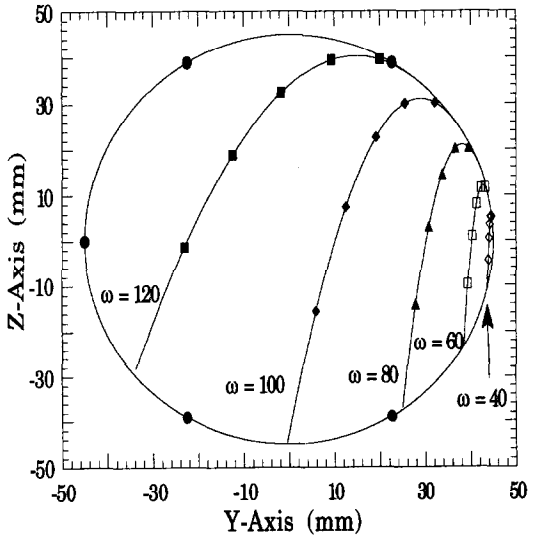

Fig. 1. Calculated flight trajectories of a 7.5 mm radius rod corresponding to different values of cylinder rotation speed. The cylinder rotation speeds are expressed in revolution per minute (rpm).

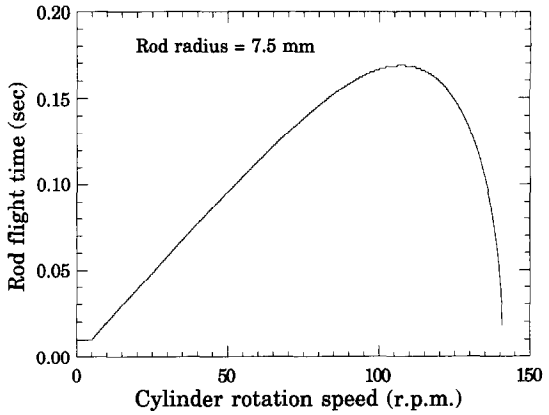

Fig. 2. Flight time variation for a rod with 7.5 mm radius as a function of the cylinder rotation speed.

Figure 1 shows the 7.5 mm radius rod trajectories for different values of cylinder rotational velocity.

Based on Fig. 1, the rod flight distance increases as function of the cylinder rotation speed "ω" to attain a maximum flight and then decreases, becoming zero for the cylinder rotational velocity greater than the critical one above which detachment cannot occur (paragraph D of the Appendix). Consequently, the flight time (obtained through computer analysis) increases with ω reaching a maximum value and then "decreases" to zero for rotational velocities greater than the critical one. Since the rod absolute velocity amplitude is a function of flight time, its variation with the cylinder rotation speed behaves similarly. Figure 2 shows the flight time variation for a rod with 7.5 mm radius as a function of the cylinder rotation speed.

Figure 3 shows the variation of the kinetic shock energy for one impact as function of the cylinder rotation speed. The calculations are appropriate for one rod.

Based on Fig. 3, we firstly remark that the kinetic shock energy increases with rod radius (the mass scales with r_d^2) and secondly that, for all rod radii, the

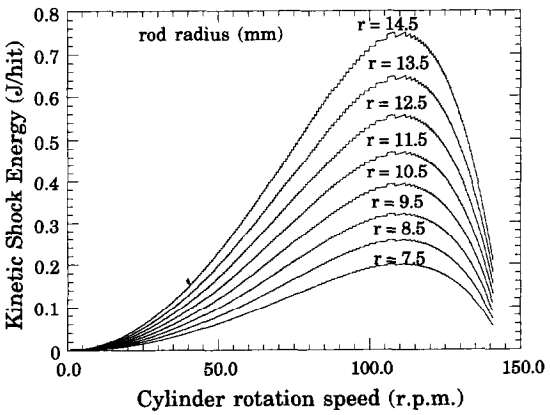

Fig. 3. Variation of the kinetic shock energy as function of the cylinder rotation speed for different rod radius values.

kinetic impact energy reaches a maximum value at an optimal cylinder rotational speed (=118.6 rpm for the physical characteristics of the used MHRM) and then decreases precipitously as the critical rotational velocity is approached.

As the dragging system allows only one shock per revolution, the shock frequency is proportional only to the cylinder rotational velocity. Consequently, the injected shock power follows the same variation as the kinetic shock energy when varying the cylinder rotation speed.

4. APPLICATION TO THE $Ni_{10}Zr_7$ COMPOUND

3.8 g of moulten spun ribbon pieces (8 mm × 10 mm × 50 μm) of mean composition $Ni_{58.8}Zr_{41.2}$ (at.%) corresponding to the $Ni_{10}Zr_7$ intermetallic compound were introduced into the mill. The mill is loaded with six steel rods (15 mm diameter, 150 mm length and 244 g mass). The cylinder is sealed with a Teflon O-ring. After 48 h of milling, the microstructural state and the phases present in the processed powder do not change. A numerical method "ABFfit program" was used to analyse the X-ray diffraction (XRD) patterns and to obtain the position and the full width at half height of the various peaks. The ball milling conditions are rod radius = 7.5 mm, ω = 118.6 rpm, f = 1.9 Hz, P_{max} = 0.38 W and $E_{k\,max}$ = 0.19 J/hit with ω the cylinder rotation speed, f the shock frequency for one rod, P_{max} the injected shock power for one rod and $E_{k\,max}$ the kinetic impact energy associated with one impact.

If the interaction between the "N" different rods does not significantly alter the individual motion of each rod the impact frequency will be N times the same frequency for an individual rod. Consequently, as six rods are used in the present work, the injected shock power will be equal to 2.29 W, i.e. 0.6 W/g for 3.8 g mass of initial elemental powder.

In studies dealing with the physics of MA in the G5 and G7 planetary ball mills [18, 19], we have previously reported that, for an injected impact power ranging from 0.4 up to 0.8 W/g, MA induces a formation of pure amorphous phase when starting from a prealloyed $Ni_{10}Zr_7$ intermetallic compound or from a mixture of $Ni_{58.8}Zr_{41.2}$ (at.%) elemental powders. Figure 4 shows the dynamic phase diagram obtained for the G5 and the G7 planetary ball mills [18, 19]. Based on this, if the injected shock power is the unique physical parameter governing the far from equilibrium phase transition as proved in [18, 19], 0.6 W/g injected shock power, developed by the so-called MHRM, will be suitable for amorphous phase formation.

Figure 5 explains the deconvolution of the [30°, 75°] angular domain (in 2θ) of the rod milled powders' XRD pattern (FeK_α radiation with λ = 0.19373 nm). Based on this figure, a superposition of two intense diffuse halos (dashed Gaussian), relative to the first and the second diffuse halo of an amorphous phase, and some weak crystalline peaks is seen. The diffuse halos are located at angular positions equal to 40.5 and 55.5° (in 2θ), respectively. Their full width at half height (FWHH) are respectively 7.2 and 10.6°. In this work, the XRD pattern is analysed by a very high performance program (ABFfit) which allows the detection of peaks having very weak intensities. In addition to only an amorphous contribution detected by a conventional program and reported in a later paper [23], we give here evidence for the existence of very small amount of crystalline contribution (non-dashed Gaussian). These crystalline peaks are relative to the $Ni_{10}Zr_7$ compound. The angular positions and the FWHH of the two diffuse halos are different from those reported by Gaffet and Yousfi [24]. The accuracy of the deconvolution of Fig. 5 is very good and all other scenarios of crystalline vs amorphous phases lead approximately to the same result. The good accuracy of the results obtained by this numerical program has been checked by Gaffet and Harmelin [25].

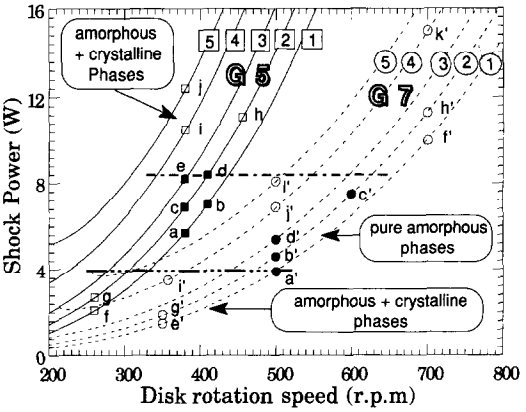

Fig. 4. Injected shock power as function of the disk and vial rotation speeds for the G5 (——) and G7 (– – –) planetary ball mills. The vial rotation speed values (in rpm) are referred by the numbers 1–5 written near each corresponding curve: 1 = 150; 2 = 250; 3 = 350; 4 = 500; and 5 = 600 rpm [18, 19].

We assume that the contact area of the impeller is not large enough to drag the six rods. Thus, the rods located far from the impeller surface undergo a rolling motion and do not contribute to the shock frequency and thus to the injected shock power. Only the rods which attain the detachment position and experience a gravitational force after detachment, affect the end product. Consequently, the injected shock power is less than 0.6 W/g and a mixture of large amount of amorphous phase and small amount of crystalline phase is obtained. So, to obtain a pure amorphous phase, we increase the impeller area in order to insure the lifting of all the rods.

We state that whatever the used device to accomplish the milling process, the injected shock power is

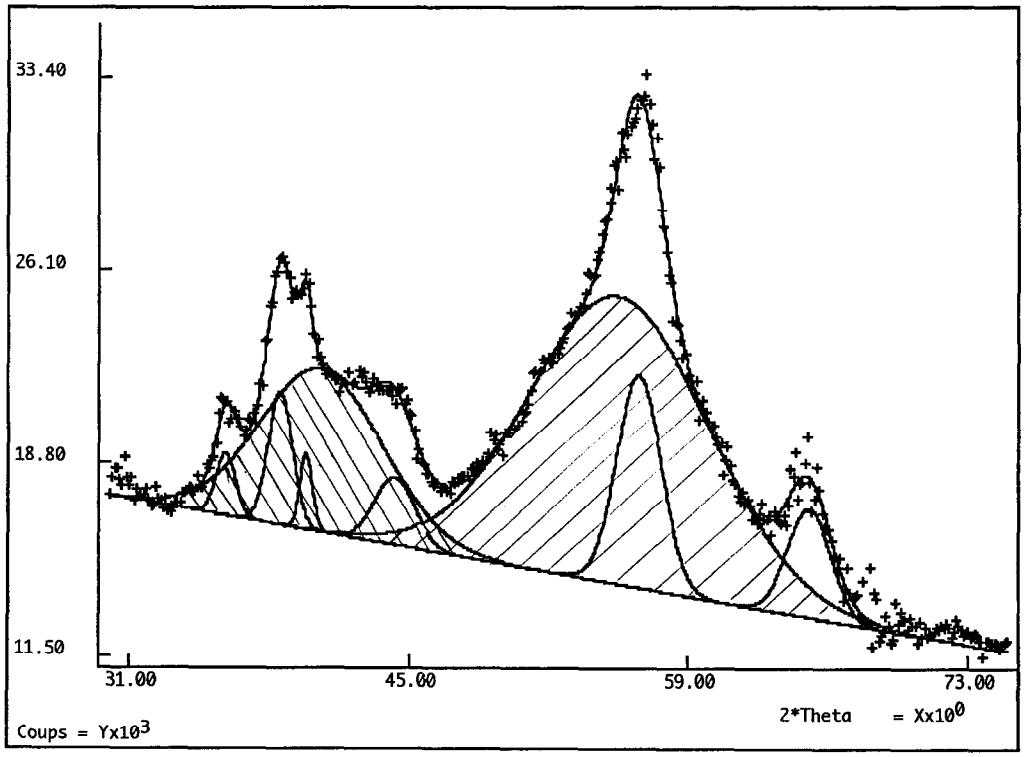

Fig. 5. Deconvolution of the rod milled power XRD pattern corresponding to a 0.6 W/g injected shock power, in an angular position ranging from 35 up to 75° (in 2θ). The initial states are formed by pre-alloyed $Ni_{10}Zr_7$ intermetallic compound. The crystalline peaks, relative to the $Ni_{10}Zr_7$ intermetallic compound, reported in the figure are [022] (35.8°), [401] (38.5°), [113] (39.8°), [402] (44.2°), [042] (56.5°) and [441] (65.0°).

the unique physical parameter governing the far from equilibrium phase transitions in mechanical alloying. In the case of the prealloyed $Ni_{10}Zr_7$ intermetallic compound, a pure amorphous phase can be formed only when the injected shock power ranges from 0.4 to 0.8 W/g.

Eckert *et al.* [26] assume that the temperature increase during mechanical alloying is a very important parameter of the process. They conclude that partial crystallisation of the formed amorphous phase can occur during mechanical alloying at high milling intensities. Thus the crystallisation of the formed amorphous phase can not simply be caused by the milling but must be an effect of excess heating during mechanical alloying. Based on the procedure proposed by Schwarz and Koch [27], they estimate the peak temperature reached within the powder particles during milling. They obtained $\Delta T = 130$, 247 and 407°C for ball milling conditions corresponding to the 3, 5 and 7 industrial setting. Since an isothermal anneal of the amorphous powders at 400°C for only 5 min is sufficient to produce partially crystallised materials with a similar X-ray diffraction pattern to that obtained for the $Ni_{70}Zr_{30}$ powder milled for 60 h at the industrial setting 7, the authors [26] conclude that the actual temperature of the individual particles during mechanical alloying can in fact be rather high—at least high enough to cause crystallisation of formed amorphous particles. Miller *et al.* [28], using microsecond time-resolved radiometry, observed temperature increases of the order of 400–500°C upon impacting NaCl crystals.

At first glance, it is important to note that these temperature rises can induce crystallisation of the phases formed during processing and that the crystalline phases obtained for high shock power values (Fig. 4) can be the result of a partial crystallisation of the formed amorphous phase due to the excess of heating as assumed in our previous works [18, 19].

Second, we assert that if the impact power is lower than a minimum value, mechanical alloying induces, after a long ball milling duration, only a refinement of the powder microstructure and an increase of the defect quantity until reaching a steady state which is not able to be destabilized into another structural state, whereas, if the impact power is greater than a minimum power value, mechanical alloying induces a refinement of the powder microstructure and an increase of the defect quantity at a rate able to induce, even in the earlier stages of MA, a mixture of structurally transformed phase and initial phase. In the later case, the steady state can result, depending on the value of the impact power, in a mixture of structurally transformed phase and initial phase or in a homogeneous structurally transformed phase.

Table 1. Documented [27] and calculated values of the kinetic energy, the shock frequency and the shock power for the G5 and G7 planetary ball mills [18, 19] and the modified horizontal rod mill (MHRM) (this work)

		Vibratory mills		Planetary ball mills			Horizontal mills
	Attritor [27]	Pulv. O [27]	SPEX [27]	Pulv. P5 [27]	G7 [18, 19]	G5 [18, 19]	MHRM (this work)
Velocity of the ball (m/s)	0–0.8	0.14–0.24	<3.9	2.5–4	0.24–6.58	0.28–11.24	0–1.247
Kinetic energy (10^{-3} J/hit)	<10	3–30	<120	10–400	0.4–303.2	0.53–884	0–190
Shock frequency (Hz)	>1000	15–50	200	~100	5.0–92.4 (5 balls)	4.5–90.7 (5 balls)	0–2.4 (1 rod)
Power (W/g/ball or rod)	<0.001	0.005–0.14	<0.24	0.01–0.8	0–0.56	0–1.604	0–0.1

The structural and microstructural states remained unchanged when the elastic energy storage in the powder becomes impossible, i.e. when the milling process can not induce more fragmentation of the powder particles and a greater increase of the defect densities.

Really only a fraction of the impact energy is consumed by the powder to achieve the phase transition. The other fraction serves to heat the powder, the ball and the vial surface, i.e. the actual power experienced by the powder scales with the shock power. The scaling constant, small compared to unity, depends only on the powder, the ball (the rod) and the vial materials and should be the same for different devices, i.e. independent of the milling device type. On this basis, the correlation between "shock power" and structure would be reasonable to be extrapolated from one device to another. So, the levels of the three domains of the dynamical phase diagram shown in Fig. 4 may translate but they do not change their shape and, whatever the shock energy consumption percent, the amorphization proceeds above a minimum power input and below a certain maximum power input.

Chen *et al.* [29], report results documented in the materials literature concerning the kinetic energy, the shock frequency and the shock power for three most common devices: the Attritor ball mill, the planetary ball mill (Fritsch "Pulverisette P5") and the vibratory grinder (e.g. SPEX Shaker mill). Table 1 gives the documented values [29] and the calculated values of the kinetic energy, the shock frequency and the shock power for the G5 and G7 planetary ball mill [18, 19] for the horizontal rod mill (this work).

Based on Table 1, the G5 shock power domain encompasses all the other devices shock power domains. Moreover, it has been reported by Martin and Gaffet [30], that the ball milling power input domain overlap some typical mechanical straining or irradiating power input domains.

5. CONCLUSIONS

Based on a mathematical treatment of the process taking place in a MHRM, and employing simplifying assumptions, the kinematic equations giving the velocity and the acceleration of a rod in the cylinder of a modified horizontal rod mill are given. The kinetic energy transferred at the collision event, the shock frequency and the shock power are also calculated.

We newly prove that whatever the used device to accomplish the milling process, the injected shock power is the unique physical parameter governing the far from equilibrium phase transitions in mechanical alloying. For the case of the prealloyed $Ni_{10}Zr_7$ intermetallic compound, a solely amorphous phase can be formed only when the injected shock power ranges from 0.4 to 0.8 W/g.

Modified, as well as conventional, horizontal rod mills are suitable for use only in a specified cylinder rotation speed domain, i.e. for cylinder rotational velocities less than those that "pin" the rods to the mill wall.

The analysis described here will be improved by taking into account the effect of rod rolling on the inner cylinder surface. Moreover, more searches of the mechanical alloying at the local level are needed to have the really released shock energy and the free energy excess in connnection with the injected shock power. This will be reported in a next paper.

Acknowledgements—Thanks are due to Dr Evan Guillaud and F. Oudc (Analyse Physico-Chimique, Université dc Technologie de Compiegne, France) for recording the X-ray diffraction patterns. Thanks are due also to the workshop staff (CECM-CNRS) for the design and realisation of the modified horizontal rod mill "MHRM". Numerical results of the shock energy, the shock frequency and the injected shock power allowed by the G5, G7, P5, P7 and MHRM mills, obtained using the computer program, are available by writing directly to our research group.

REFERENCES

1. *Int. Symp. Mech. Alloying Kyoto, Japan* (edited by P. H. Shingu). Trans. Tech. Publications (1991). *Solid-State*

Amorphizing Transformations (organised by R. B. Schwarz and W. L. Johnson). Los Alamos, U.S.A. (1987). *Symp. Int. Amorphization by Solid-State Reaction* (organised by A. R. Yavari, E. Gaffet, J. M. Legresy and F. Bordeaux). Grenoble, France (1990). *ASM Int. Conf.* (organised by F. H. Froes and J. J. Debarbadillo). Myrtle beach, S.C., U.S.A. (1990). *European Workshop on Ordering and Disordering* (organised by A. R. Yavari and P. Desre). Grenoble, France (1991). *Int. Symp. on Metastable, Mechanically Alloyed and Nanocrystalline Materials, European Meeting on Disordering and Amorphization* (organised by A. R. Yavari). Grenoble, France (1994).

2. E. Gaffet, C. Louison, M. Harmelin and F. Faudot, *Mater. Sci. Engng* **A134,** 1380 (1991).
3. J. Kuyama, K. N. Ishihara and P. H. Singu, *Mater. Sci. For.* **88–90,** 521 (1992).
4. E. Gaffet, F. Faudot and M. Harmelin, *J. All. Comp.* **194,** 23 (1993).
5. F. Faudot, E. Gaffet and M. Harmelin, *J. Mater. Sci.* **28,** 2669 (1993).
6. C. Suryanarayana and R. Sundaresan, *Mater. Sci. Engng* **A131,** 237 (1991).
7. C. Kuhrt and L. Schultz, *J. appl. Phys.* **73,** 1975 (1993).
8. M. Abdellaoui, T. Barradi and E. Gaffet, *J. All. Comp.* **198,** 155 (1993).
9. M. Abdellaoui, T. Barradi, F. Faudot and E. Gaffet, *IEEE Trans. Magnet.*, Vol. 30, p. 4887. Presented in the 6th Joint MMM Intermag Conference, Albuquerque, New Mexico (1994).
10. E. Gaffet, N. Malhouroux and M. Abdellaoui, *J. All. Comp.* **194,** 339 (1993).
11. D. R. Maurice and T. H. Courtney, *Metall. Trans.* **21A,** 289 (1990).
12. T. H. Courtney and D. R. Maurice, *Solid State Powder Processing* (edited by A. H. Clauer and J. J. deBarbadillo). The Minerals & Materials Society (1990).
13. D. R. Maurice and T. H. Courtney, *Metall. Mater. Trans.* **25A,** 147 (1994).
14. T. H. Courtney, J. C. Malzahn Kampe, J. K. Lee and D. R. Maurice, *Diffusion Analysis and Applications* (edited by A. D. Romig Jr and M. A. Dayananda). The Minerals, Metals & Materials Society (1989).
15. R. W. Rydin, D. Maurice and T. H. Courtney, *Metall. Trans.* **24A,** 175 (1993).
16. N. Burgio, A. Iasonna, M. Magini, S. Martelli and F. Padella, *Il Nuovo Cimento* **13D,** 459.
17. M. Magini, *Mater. Sci. For.* **88–90,** 121 (1992).
18. M. Abdellaoui and E. Gaffet, *J. All. Comp.* **209,** 351 (1994).
19. M. Abdellaoui and E. Gaffet, *Acta metall. mater.* **43,** 1087 (1995).
20. P. G. McCormick, H. Huang, M. P. Dallimore, J. Diang and J. Pan, *Proc. 2nd Int. Conf. Struct. Applic. Mech. Alloying* (edited by J. J. de Barbadillo, F. H. Froes and R. Schwaez), pp. 45–50. ASM, Vancouver (1993).
21. P. Le Brun, L. Froyen and L. Delaey, *Mater. Sci. Engng* **A161,** 75 (1993).
22. A. Calka and J. S. Williams, *Mater. Sci. For.* **88–90,** 787 (1992).
23. M. Abdellaoui and E. Gaffet, *Int. Symp. on Metastable, Mechanically Alloyed and Nanocrystalline Materials, European Meeting on Disordering and Amorphization* (organised by A. R. Yavari). Grenoble, France (1994).
24. E. Gaffet and L. Yousfi, *Mater. Sci. For.* **88–90,** 51 (1992).
25. E. Gaffet and M. Harmelin, *J. Less-Common Met.* **157,** 201 (1990).
26. J. Eckert, L. Schultz, E. Hellstern and K. Urban, *J. appl. Phys.* **64,** 3224 (1988).
27. R. B. Schwarz and C. C. Koch, *Appl. Phys. Lett.* **49,** 146 (1986).
28. P. J. Miller, C. S. Coffey and V. F. Devost, *J. appl. Phys.* **59,** 913 (1986).
29. Y. Chen, R. Le Hazif and G. Martin, *Solid State Phen.* **23 & 24,** 271 (1992).
30. G. Martin and E. Gaffet, *Coll. Phys. Coll. C4 (supplément au No. 14, Tome)* **51,** 71 (1990).

APPENDIX

(A) References and "M" Point Position Expression

Figure A1 shows the rod position M at time t with, R = the cylinder radius (m), r = the rod radius (m), m = the rod mass (kg), M, a material point representing the rod position in the cylinder, $\theta = \omega t$, the cylinder rotation angle with $\boldsymbol{\omega} = \omega\mathbf{I}$, $(O, \mathbf{I}, \mathbf{J}, \mathbf{K})$ a direct Cartesian referential and $(O, \mathbf{U}_\rho, \mathbf{U}_\theta)$ a cylindrical referential such that $\mathbf{U}_\rho // \mathbf{R}$ and $\mathbf{U}_\theta \perp \mathbf{U}_\rho$. Based on Fig. A1

$$\mathbf{OM} = R\mathbf{U}_\rho. \tag{A1}$$

$$\mathbf{OM} = R[\cos(\theta)\mathbf{J} + \sin(\theta)\mathbf{K}]. \tag{A2}$$

(B) Calculation of the Absolute Velocity and the Absolute Acceleration

The absolute velocity $\mathbf{V}_a$ of the point M is given as follows

$$\mathbf{V}_a = \frac{d(\mathbf{OM})}{dt} = \frac{d[R(\cos(\theta)\mathbf{J} + \sin(\theta)\mathbf{K})]}{dt} \tag{B1}$$

$$\mathbf{V}_a = \frac{dR}{dt}[\cos(\theta)\mathbf{J} + \sin(\theta)\mathbf{K}] + R\frac{d\theta}{dt}[-\sin(\theta)\mathbf{J} + \cos(\theta)\mathbf{K}]. \tag{B2}$$

Thus, as $dR/dt = 0$ and $d\theta/dt = \omega$, the expression of the absolute velocity is simplified to

$$\mathbf{V}_a = R\omega[-\sin(\theta)\mathbf{J} + \cos(\theta)\mathbf{K}] \tag{B3}$$

or as $\mathbf{U}_\theta = -\sin(\theta)\mathbf{J} + \cos(\theta)\mathbf{K}$, the final expression of the absolute velocity is given by

$$\mathbf{V}_a = R\omega\mathbf{U}_\theta. \tag{B4}$$

The absolute acceleration γ_a of the point M, obtained by the derivative of its absolute velocity $\mathbf{V}_a$ with respect to time, is given as follows

$$\gamma_a = \frac{d(\mathbf{V}_a)}{dt} = \frac{d(R\omega\mathbf{U}_\theta)}{dt} \tag{B5}$$

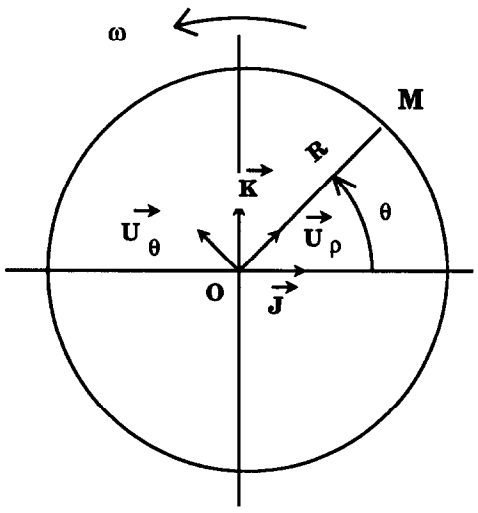

Fig. A1. Geometry of the MHRM seen from the side. The various vectors and angles are explained in the text.

as R and ω are constant, expression (B5) will be simplified as

$$\gamma_a = R\omega \frac{d[-\sin(\theta)\mathbf{J} + \cos(\theta)\mathbf{K}]}{dt} \quad \text{(B6)}$$

$$\gamma_a = R\omega \frac{d\theta}{dt}[-\cos(\theta)\mathbf{J} - \sin(\theta)\mathbf{K}] \quad \text{(B7)}$$

as $\mathbf{U}_\rho = \cos(\theta)\mathbf{J} + \sin(\theta)\mathbf{K}$ and $d\theta/dt = \omega$, the final expression of the absolute acceleration is given as

$$\gamma_a = -R\omega^2\mathbf{U}_\rho. \quad \text{(B8)}$$

(C) Decomposition of the Impeller and the Cylinder Reactions

Figure A2 shows the front view and the left side view of the modified horizontal rod mill (MHRM) with

(1) the cylinder
(2) impeller permitting the "lifting" of the rod (lifting system)
(3) the rod used
(4) two covers on which are attached the impellers (one to each cover).

Based on this figure, the expression of the cylinder and the impeller reaction $\mathbf{R}$ and the rod weight as function of the $\mathbf{U}_\rho$ and $\mathbf{U}_\theta$ vectors is given as follows

$$\mathbf{R} = \mathbf{R}_\rho + \mathbf{R}_\theta \quad \text{(C1)}$$

$$\mathbf{P} = \mathbf{P}_\rho + \mathbf{P}_\theta \quad \text{(C2)}$$

with $\mathbf{R}_\rho = -R_\rho\mathbf{U}_\rho$ the cylinder reaction, $\mathbf{R}_\theta = R_\theta\mathbf{U}_\theta$ the impeller reaction, $\mathbf{P}_\rho = -mg\cos(\pi/2 - \theta)\mathbf{U}_\rho$ the normal component of the rod weight and $\mathbf{P}_\theta = -mg\sin(\pi/2 - \theta)\mathbf{U}_\theta$ the tangential component of the rod weight ($R_\rho, R_\theta \geq 0$).

(D) Condition of Permanent Sticking of the Rod on the Inner Cylinder Surface

We now assume that no detachment occurs up to an angular rod position θ such that $\theta = \pi/2$. In this case, the $\mathbf{U}_\rho$ vector will be equal to the $\mathbf{K}$ vector and, taking into account the finite rod radius, equation (8) will be written as

$$\mathbf{R}_\rho + m((R - r)\omega^2 - g)\mathbf{K} = \mathbf{0}. \quad \text{(D1)}$$

Suppose now that $(R - r)\omega^2 > g$. In this case, the effective centrifugal force $m((R - r)\omega^2 - g)\mathbf{K}$ always exceeds zero and consequently no detachment event occurs. Thus, if the cylinder rotation speed is greater than a critical value equal to $\sqrt{g/R - r}$, the rod remains "stuck" to the cylinder inner surface and no collision event can happen. So, we show that in distinction to the planetary ball mill, the modified horizontal rod mill (MHRM) is fruitful only for a specified cylinder rotational velocity range.

(E) Cartesian Expression of the Detachment Velocity and Detachment Acceleration

The expression of the absolute rod velocity is given by equation (B3). Taking into account that the detachment event occurs when the rod position θ is such that $\sin(\theta_d) = (R - r)\omega^2/g$, the expression for the detachment velocity $\mathbf{V}_d$ is given as

$$\mathbf{V}_d = -(R - r)\omega\sin(\theta_d)\mathbf{J} + (R - r)\omega\cos(\theta_d)\mathbf{K}. \quad \text{(E1)}$$

The detachment velocity can be decomposed into two components $\mathbf{V}_{dy}$ (along the Y axis) and $\mathbf{V}_{dz}$ (along the Z axis) such that

$$\mathbf{V}_{dy} = -(R - r)\omega\sin(\theta_d)\mathbf{J}$$

and

$$\mathbf{V}_{dz} = (R - r)\omega\cos(\theta_d)\mathbf{K}. \quad \text{(E2)}$$

The vectorial position rode above the detachment event is given by equation (A2). At the detachment event, and taking into account the rod radius, the vectorial M point position $\mathbf{OM}_d$ is

$$\mathbf{OM}_d = (R - r)[\cos(\theta_d)\mathbf{J} + \sin(\theta_d)\mathbf{K}]. \quad \text{(E3)}$$

This position can be decomposed into two components $\mathbf{OM}_{dy}$ (along the Y axis) and $\mathbf{OM}_{dz}$ (along the Z axis) such that

$$\mathbf{OM}_{dy} = (R - r)\cos(\theta_d)\mathbf{J}$$

and

$$\mathbf{OM}_{dz} = (R - r)\sin(\theta_d)\mathbf{K}. \quad \text{(E4)}$$

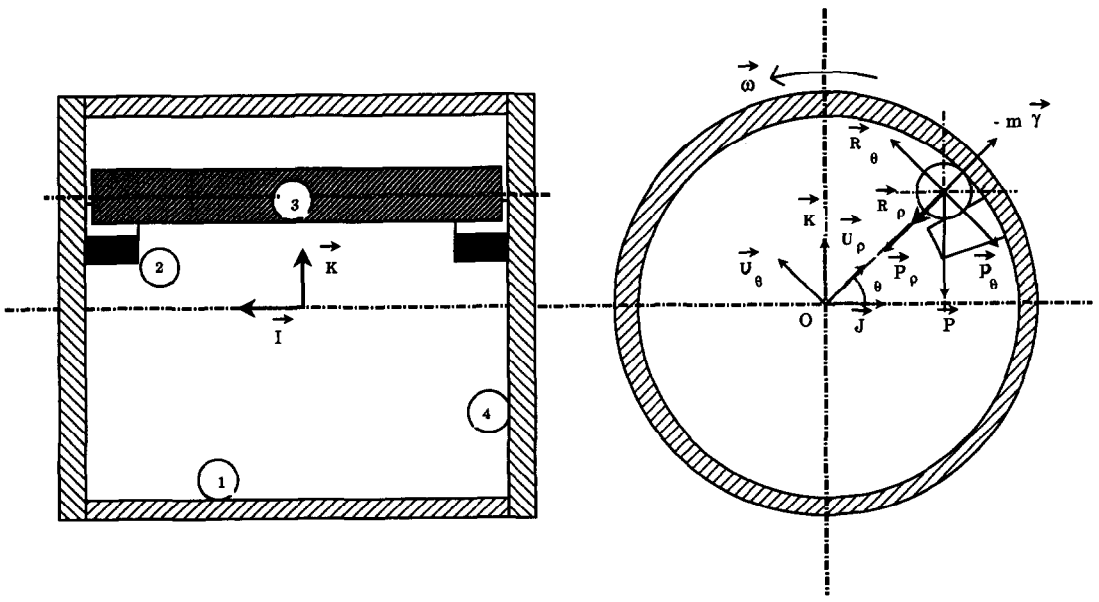

Fig. A2. Front view and left side view of the MHRM.

(F) Calculation of the Impact Velocity

The collision velocity $\mathbf{V}_c$ is given by the derivation of the rod vector position **OM** after the detachment event. It can be decomposed into two components: $\mathbf{V}_{(Y,t)}$ along the Y axis and $\mathbf{V}_{(Z,t)}$ along the Z axis such as

$$\mathbf{V}_{(Y,t)} = \frac{dy}{dt}\mathbf{J} = -(R-r)\omega \sin(\theta_d)\mathbf{J} \tag{F1}$$

$$\mathbf{V}_{(Z,t)} = \frac{dz}{dt}\mathbf{K} = [-gt + (R-r)\omega \cos(\theta_d)]\mathbf{K}. \tag{F2}$$

At the t_c time corresponding to the collision event, amplitude of the collision velocity is given by

$$\|\mathbf{V}_c\| = \sqrt{\|\mathbf{V}_{(Y,t_c)}\|^2 + \|\mathbf{V}_{(Z,t_c)}\|^2} \tag{F3}$$

$$\|\mathbf{V}_c\| = \sqrt{[(R-r)\omega \sin(\theta_d)]^2 + [-gt_c + (R-r)\omega \cos(\theta_d)]^2}. \tag{F4}$$